Draft version February 1, 2017
Preprint typeset using LaTeX style emulateapj v. 5/2/11

arXiv:1701.08987v1 [astro-ph.SR] 31 Jan 2017

SEISMIC MEASUREMENT OF THE LOCATIONS OF THE BASE OF CONVECTION ZONE AND HELIUM IONIZATION ZONE FOR STARS IN THE *KEPLER* SEISMIC LEGACY SAMPLE

Kuldeep Verma[1,2,3], Keyuri Raodeo[4], H. M. Antia[2], Anwesh Mazumdar[4], Sarbani Basu[5], Mikkel N. Lund[6,1], Víctor Silva Aguirre[1]

Draft version February 1, 2017

ABSTRACT

Acoustic glitches are regions inside a star where the sound speed or its derivatives change abruptly. These leave a small characteristic oscillatory signature in the stellar oscillation frequencies. With the precision achieved by *Kepler* seismic data, it is now possible to extract these small amplitude oscillatory signatures, and infer the locations of the glitches. We perform glitch analysis for all the 66 stars in the *Kepler* seismic LEGACY sample to derive the locations of the base of the envelope convection zone and the helium ionization zone. The signature from helium ionization zone is found to be robust for all stars in the sample, whereas the convection zone signature is found to be weak and problematic, particularly for relatively massive stars with large errorbars on the oscillation frequencies. We demonstrate that the helium glitch signature can be used to constrain the properties of the helium ionization layers and the helium abundance.

Subject headings: stars: fundamental parameters — stars: interiors — stars: oscillations — stars: solar-type

1. INTRODUCTION

An accurate understanding of stellar structure and evolution is of paramount importance to astrophysics, and physics in general. Indeed, the properties of stars are used to infer the nature of the associated exoplanets and to learn the history of the Milky Way. Seismic data from *CoRoT* (Baglin 2006; Baglin et al. 2009) and *Kepler* (Borucki et al. 2009; Koch et al. 2010) space missions have revolutionized our understanding of stellar structure. The precise set of observed oscillation frequencies are being used to test the various hypotheses of stellar physics.

It had been proposed that the signatures of the acoustic glitches in the oscillation frequencies of distant stars could be used to determine the depths of the base of the envelope convection zone and helium ionization zone (Monteiro et al. 2000; Mazumdar & Antia 2001; Gough 2002; Roxburgh & Vorontsov 2003). The amplitude of the glitch signature is a few orders of magnitude smaller than the background smooth component, and a set of precise oscillation frequencies are required in a sufficiently large frequency range to use this technique. With the availability of the high quality seismic data from *CoRoT* and *Kepler* space missions, it has become possible to apply this technique to distant stars. Miglio et al. (2010) used the modulation of the frequency separation observed in *CoRoT* data to determine the location of the helium ionization zone in a red giant. Similarly, Mazumdar et al. (2012) used *CoRoT* data for HD49933 to determine the acoustic depths of the helium ionization zone and base of the envelope convection zone (see also, Mazumdar et al. 2011; Roxburgh 2011). Mazumdar et al. (2014) performed a more extensive study using data from about a year of observations by *Kepler* for 19 stars to determine the acoustic depths of both glitches. In this work, we extend the study to 66 stars using *Kepler* data, covering up to 3.5 years of observations. Apart from location, the oscillatory signal from the helium ionization zone was shown to be sensitive to the envelope helium abundance (Basu et al. 2004; Monteiro & Thompson 2005; Houdek & Gough 2007). Verma et al. (2014b) have used oscillation frequencies from *Kepler* to determine the envelope helium abundance of a binary system, 16 Cyg A & B.

The independent measurement of the locations of the base of the convection zone and helium ionization zone can be used to constrain the stellar properties better. The fundamental stellar parameters are not only useful in the context of stellar evolution but also in the studies of exoplanets (see, e.g., Nutzman et al. 2011; Gilliland et al. 2013; Liu et al. 2014; Silva Aguirre et al. 2015), stellar populations (Chaplin et al. 2011), and galactic archeology (see, e.g., Miglio et al. 2013; Casagrande et al. 2014, 2016). The stellar ages are particularly important, and cannot be determined directly. The standard technique to determine stellar age compares the observed surface properties of the star with the corresponding quantities from the stellar evolution models. This approach is effective in determining the ages of stellar clusters, provided the observed sample includes stars at different evolutionary stages, including those beyond the main-sequence. But for the isolated field stars, we need ad-

kuldeep@phys.au.dk
[1] Stellar Astrophysics Centre, Department of Physics and Astronomy, Aarhus University, Ny Munkegade 120, DK-8000 Aarhus C, Denmark
[2] Tata Institute of Fundamental Research, Homi Bhabha Road, Mumbai 400005, India
[3] Centre for Excellence in Basic Sciences, University of Mumbai, Kalina, Mumbai 400098, India
[4] Homi Bhabha Centre for Science Education, TIFR, V. N. Purav Marg, Mankhurd, Mumbai 400088, India
[5] Astronomy Department, Yale University, P. O. Box 208101, New Haven, CT 065208101, USA
[6] School of Physics and Astronomy, University of Birmingham, Edgbaston, Birmingham, B15 2TT, UK

ditional seismic constraints to determine the ages reliably. For instance, the observed oscillation frequencies or their appropriate combinations along with spectroscopic data are used to obtain the best-fit stellar model (see, e.g., Mathur et al. 2012; Chaplin et al. 2014; Metcalfe et al. 2014; Silva Aguirre et al. 2015). Recently, Silva Aguirre et al. (2013) have obtained stellar ages to about 10% accuracy using seismic data in addition to spectroscopic observations. The process of determining the best-fit stellar model typically involves minimization of a cost function, which is a highly nonlinear function and may have multiple minima (see, e.g., Aerts et al. 2010), and in some cases two or more minima may be close in terms of the quality of the fits. The additional information from the acoustic glitches can be used to resolve these near degeneracies.

The locations of the acoustic glitches can also be used to constrain the input physics of the stellar evolution models. This was demonstrated by Mazumdar (2005) using synthetic data for a *CoRoT* target star. The evolutionary models require the heavy element abundance, Z, of the star, which is generally derived from the observed [Fe/H] assuming the relative abundances to be similar to the solar abundances. The recent revision of the solar heavy element abundances using 3D hydrodynamic model for the solar atmosphere (Asplund et al. 2009) are known to be inconsistent with the helioseismic constraints (Basu & Antia 2008; Gough 2013, and references therein), while the earlier solar abundance tables of Grevesse & Sauval (1998), obtained using 1D solar atmospheric model, provide better agreement. Recent measurements of iron opacity in a condition similar to the solar interior shows that the iron opacity used in stellar models are significantly low (see, Bailey et al. 2015). This may partly resolve the issue of solar abundance problem, but not completely. It would be interesting to see if the asteroseismic data can tell us whether the problem is with opacities, or solar abundances, or with both (see, e.g., Mazumdar et al. 2010). The position of the base of the convection zone is very sensitive to the opacity of the stellar material, which also depends on the abundance of the heavy elements, and can throw some light on the above issues.

Lund et al. (2016) have recently determined the oscillation frequencies of 66 main-sequence stars for which there are more than one year of *Kepler* data. This sample is known as *Kepler* seismic LEGACY sample. Silva Aguirre et al. (2016) have used these set of frequencies to derive the properties of all stars in the sample. They found the masses, radii, and the ages with average uncertainties of about 4%, 2%, and 10%, respectively. The long duration of the observations ensures sufficient precision to study the acoustic glitches in these stars. In this work, we use the above set of oscillation frequencies for all the 66 stars to estimate the acoustic depths of the base of the convection zone and helium ionization zone. We extend the work of Silva Aguirre et al. (2016) by including the additional observables obtained from the glitch analysis to our stellar model fitting.

The rest of the paper is organized as follows: Section 2 describes the spectroscopic and seismic data used in the study, the techniques to fit the glitch signature are described in Section 3, Section 4 presents the procedure to get the best-fit model, the results of the glitch analysis and stellar model fitting are discussed in Section 5, Section 6 demonstrates the importance of the glitch analysis in stellar model fitting, and finally we summarize the conclusions of this study in Section 7.

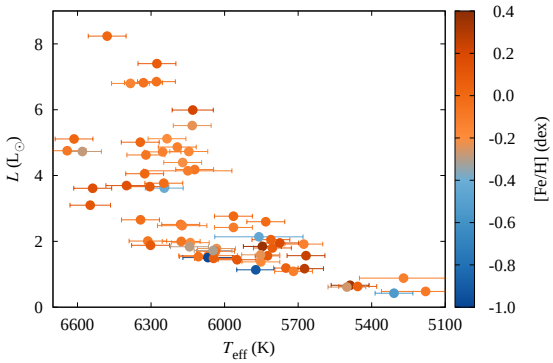

FIG. 1.— Hertzsprung-Russell diagram showing the parameter space covered by the LEGACY sample. The luminosity of stars was obtained from the best-fit model. The colors represent the observed surface metallicity of the star.

2. SPECTROSCOPIC AND SEISMIC DATA

NASA's *Kepler* space mission has observed solar-like oscillations in over hundred Sun-like main-sequence stars. The LEGACY sample consists of 66 main-sequence stars observed in short cadence mode for at least 12 months (most of the stars have a time series of approximately 3 years), and spans a large range in metallicity. Figure 1 shows the locations of the stars in the Hertzsprung-Russell diagram. We used the spectroscopic and seismic data from Lund et al. (2016), and refer the reader to that paper for the details on the target selection, compilation of the spectroscopic data, and the computation of the stellar oscillation frequencies (see also, Silva Aguirre et al. 2016).

3. FITTING TECHNIQUES

Acoustic glitches inside a star are regions where the sound speed or its derivatives show an abrupt variation on length scales shorter than the typical wavelengths of the acoustic modes. Such glitches introduce an oscillatory component, $\delta\nu_{\rm g}$, in the frequencies of stellar oscillations as a function of the radial order, n, of the form, $\delta\nu_{\rm g}(\nu) \propto \sin(4\pi\tau_{\rm g}\nu + \psi_{\rm g})$, where $\tau_{\rm g}$ is the acoustic depth of the glitch (see, Gough & Thompson 1988; Vorontsov 1988; Gough 1990), and ψ_g is the phase of the oscillatory signal.

The two main sources of acoustic glitches in a Sun-like main-sequence star are the base of the envelope convection zone (CZ) where the second derivative of the sound speed, c, is discontinuous, and the helium (He) ionization zone where the first adiabatic index, Γ_1, varies rapidly. Both of these glitches lie deep inside the star where the non-adiabatic effects are weak, and the glitch signatures are not significantly affected by the poorly understood near-surface layers. The boundary of the core convection zone does not contribute a significant oscillatory signal as this is aliased to a signal with a very small acoustic depth (Mazumdar & Antia 2001), and that cannot be distinguished from the background smooth component of the frequency. It was customarily believed that the oscillatory signal from the helium ionization zone arises

from the dip in Γ_1-profile in the second helium ionization zone. The fitted acoustic depth of the helium signal was, however, found to be significantly smaller than the depth of the He II ionization zone, and Houdek & Gough (2007) attributed this difference to the neglect of the acoustic cut-off frequency in the phase function and the signal from the He I ionization zone. Broomhall et al. (2014) found that the fitted acoustic depth of the helium signal in the models of the red-giants agrees with the acoustic depth of the peak in Γ_1-profile between the He I and He II ionization zones. Verma et al. (2014a) did a detailed study of glitch signals from various ionization zones of helium in main-sequence stellar models to find that the fitted acoustic depth always matches that of the peak in Γ_1 between the two ionization zones. Their attempt to fit the signatures from both ionization zones of helium resulted in a significantly better fit for the solar oscillation frequencies, but the fit was again to the usual peak between the two helium ionization zones, and a peak above the hydrogen ionization zone. More significantly, the inclusion of the second glitch did not affect the parameters for the helium glitch (the glitch between the two helium ionization zones). Hence in this work, we fit the glitch signature from the helium ionization zone only.

The amplitudes of the oscillatory signature from the acoustic glitches are approximately three or more orders of magnitude smaller than the background smooth component, which makes it hard to extract them from the stellar oscillation frequencies. There are two popular approaches to extract the glitch signatures: the first attempts to fit the oscillation frequencies directly, while the second tries to fit the second differences of the oscillation frequencies. We use both fitting methods, Method A and Method B as described below, to derive the glitch parameters. The two independent methods can be used to assess the associated systematic uncertainties in the estimated glitch properties.

3.1. *Fitting frequencies directly (Method A)*

There are again two different approaches to extract the glitch signatures from the stellar oscillation frequencies: the first removes the smooth component from the frequencies as a function of radial order, n, and fits the residual (see, e.g., Monteiro et al. 1994; Monteiro & Thompson 1998; Monteiro et al. 2000), while the second approach fits the smooth component and the glitch signals simultaneously (see, e.g., Verma et al. 2014b,a). We have used the second approach in this work as described below.

We model the smooth component of the oscillation frequency using a l-dependent fourth degree polynomial in the radial order, n, where l is the harmonic degree. The functional forms of the glitch signatures are adapted from Houdek & Gough (2007). We fit the oscillation frequency, $\nu_{n,l}$, to the function,

$$f(n,l) = P_l(n) + \frac{a_c}{\nu^2}\sin(4\pi\tau_{\rm CZ}\nu + \psi_{\rm CZ}) + a_h\nu e^{-c_2\nu^2}\sin(4\pi\tau_{\rm He}\nu + \psi_{\rm He}), \quad (1)$$

where $P_l(n) = \sum_{i=0}^{4} a_i(l) n^i$ is the contribution of the smooth component with $a_i(l)$ being the coefficients of the polynomial. The second term is the oscillatory contribution coming from the base of the convection zone with a_c related to the amplitude, $\tau_{\rm CZ}$ being the acoustic depth of the base of the convection zone, and $\psi_{\rm CZ}$ being the phase of the signal. The third term is the oscillatory contribution coming from the helium ionization zone with a_h related to the amplitude, c_2 related to the width of Γ_1-peak between the He I and He II ionization zones, $\tau_{\rm He}$ being the acoustic depth of the Γ_1-peak, and $\psi_{\rm He}$ being the phase. This function contains a total of 22 free parameters when fitting $l = 0$, 1, and 2 modes ($5 \times 3 = 15$ polynomial coefficients $a_i(l)$, a_c, $\tau_{\rm CZ}$, $\psi_{\rm CZ}$, a_h, c_2, $\tau_{\rm He}$, $\psi_{\rm He}$).

To determine the parameters of Eq. (1), we perform a regularized least-squares fit by minimizing the function,

$$\chi^2_{\rm g} = \sum_{n,l}\left[\frac{\nu_{n,l} - f(n,l)}{\sigma_{n,l}}\right]^2 + \lambda^2 \sum_{n,l}\left[\frac{d^3 P_l(n)}{dn^3}\right]^2, \quad (2)$$

where $\sigma_{n,l}$ is the quoted uncertainty on the observed $\nu_{n,l}$ and λ is the regularization parameter. Note that we have used a third derivative regularization instead of the second derivative used in Verma et al. (2014b,a). The third derivative regularization marginally improves the stability of the fit. The regularization parameter is determined in the same way as in Verma et al. (2014b) for the solar oscillation frequencies, and the same value is used for stars in the *Kepler* LEGACY sample. The cost function $\chi^2_{\rm g}$ defined in Eq. (2) is a nonlinear function of the fitting parameters, hence the fit may not converge to the global minimum, particularly if the initial guess is not close enough. We search for the global minimum in a subspace of the parameter space by repeating the fitting process for 100 sets of randomly chosen initial guesses. The fit with minimum value of the standard chi-square (first term in Eq. 2) among 100 trials is accepted as the best fit. We generate 1,000 realizations of the observed oscillation frequencies assuming the uncertainties on them are uncorrelated and normally distributed. We fit all the realizations to get the distributions of the fitted parameters. The median of the distribution is accepted as the parameter value while the $16^{\rm th}$ and $84^{\rm th}$ percentiles of the distribution give the negative and positive errorbars.

The oscillatory signature from the base of the convection zone is typically weak with the amplitude of the order of the errors on the oscillation frequencies. Consequently, the distribution of the fitted parameters may have multiple peaks. We use only those realizations for which the fitted acoustic depth falls in the dominant peak to calculate the median and error estimates. The parameters associated with the CZ signature may not be correct due to the problem of aliasing (Mazumdar & Antia 2001), in which case the fitted acoustic depth is found to be the complement of $\tau_{\rm CZ}$, i.e., $\tau = T_0 - \tau_{\rm CZ}$ (where T_0 is the acoustic radius of the star). In spite of the problem of aliasing, the glitch analysis is useful as it can restrict $\tau_{\rm CZ}$ from its infinite possible values to two numbers, viz., $\tau_{\rm CZ}$ and $T_0 - \tau_{\rm CZ}$. In some cases, particularly for relatively massive stars with large errorbars on the oscillation frequencies, there may not be any well defined peak in the distribution of the fitted parameters for the convection zone signal, as the values may be spread over a wide interval.

3.2. *Fitting second differences (Method B)*

This is a well known method for extracting the signatures of the acoustic glitches from the observed stellar oscillation frequencies (see, e.g., Gough 1990; Basu et al. 1994, 2004). The oscillation frequencies follow closely the asymptotic expression of Tassoul (1980), which predominantly depends linearly on the radial order for a given degree. Hence taking the second difference of the oscillation frequency with respect to n,

$$\delta^2\nu_{n,l} := \nu_{n-1,l} - 2\nu_{n,l} + \nu_{n+1,l}, \tag{3}$$

reduces the background smooth component significantly. This, however, complicates slightly the fitting procedure because the differences have correlated errorbars, and the covariance matrix has to be used in the definition of the chi-square to be minimized.

We fit the second differences of the oscillation frequencies to the following function adapted from Houdek & Gough (2007),

$$\delta^2\nu = a_0 + a_1\nu + \frac{b_0}{\nu^2}\sin(4\pi\nu\tau_{\rm CZ} + \phi_{\rm CZ}) + c_0\nu e^{-c_2\nu^2}\sin(4\pi\nu\tau_{\rm He} + \phi_{\rm He}), \tag{4}$$

where the first two terms take care of the residual smooth component left after the second differences are calculated; the third term is the oscillatory contribution coming from the base of the convection zone with b_0 related to the amplitude, $\tau_{\rm CZ}$ being the acoustic depth of the base of the convection zone, and $\phi_{\rm CZ}$ being the phase; the fourth term is the oscillatory contribution coming from the helium ionization zone with c_0 related to the amplitude, c_2 related to the width of Γ_1-peak between the He I and He II ionization zones, $\tau_{\rm He}$ being the acoustic depth of the Γ_1-peak, and $\phi_{\rm He}$ being the phase. The above amplitudes of the oscillatory signatures in the second differences may be converted to the corresponding amplitudes in the oscillation frequencies by dividing them with $4\sin^2(2\pi\tau_{\rm g}\langle\Delta\nu\rangle)$(see, Basu et al. 1994), where $\langle\Delta\nu\rangle$ is the average large frequency separation.

We fit the second differences of the oscillation frequencies to the function defined in Eq. (4) to determine the parameters a_0, a_1, b_0, $\tau_{\rm CZ}$, $\phi_{\rm CZ}$, c_0, c_2, $\tau_{\rm He}$, and $\phi_{\rm He}$. We again search for the global minimum as in Method A with 100 trials on the initial guesses. The parameter values and the associated errorbars are computed using the distribution of the parameters obtained by fitting 10,000 realizations of the observed oscillation frequencies. The CZ signature has the same limitations as those discussed in the context of Method A.

4. BEST-FIT MODELS

We modeled each star in three different ways using various methods and evolutionary codes. The approaches are briefly described below.

4.1. *MESA models*

We used the Modules for Experiments in Stellar Astrophysics code (MESA; Paxton et al. 2011, 2013) for stellar modeling. This code can be used with various input physics and data tables. We used the OPAL equation of state (Rogers & Nayfonov 2002), Opacity Project (OP) high-temperature opacities (Badnell et al. 2005; Seaton 2005) supplemented with low-temperature opacities from Ferguson et al. (2005). The metallicity mixtures from Grevesse & Sauval (1998) was used. We used reaction rates from NACRE (Angulo et al. 1999) for all reactions except $^{14}{\rm N}(p,\gamma)^{15}{\rm O}$ and $^{12}{\rm C}(\alpha,\gamma)^{16}{\rm O}$, for which updated reaction rates from Imbriani et al. (2005) and Kunz et al. (2002) were used. Convection was modeled using the standard mixing-length theory (Cox & Giuli 1968). An exponential overshoot (Herwig 2000) was included for stars with masses greater than 1.10 $M_\odot$. The diffusion of helium and heavy elements was incorporated for stars of masses less than 1.35 $M_\odot$ using the prescription of Thoul et al. (1994). For higher mass stars, the diffusion prescription clearly overestimates the settling of helium and heavy elements in the envelope, and hence was not used. The adiabatic oscillation frequencies were calculated using the Adiabatic Pulsation code (ADIPLS; Christensen-Dalsgaard 2008).

We constructed models independently for each star in the LEGACY sample on a mesh of stellar parameters—the mass M, initial helium abundance Y_i, initial metallicity $[{\rm Fe/H}]_i$, mixing-length $\alpha_{\rm MLT}$, and the overshoot parameter $\alpha_{\rm OV}$. We generated 1,000 to 2,000 randomly distributed mesh points for an individual star in a reasonable subspace of the parameter space (we start with a chosen subspace with 1,000 mesh points, and extend it uniformly if the best-fit model falls near the edge). The models corresponding to every mesh point were evolved until the track enters in a box formed by the 4σ uncertainties in the observed effective temperature $T_{\rm eff}$, surface metallicity [Fe/H], and average large frequency separation $\langle\Delta\nu\rangle$. We fitted the surface corrected model frequencies (Kjeldsen et al. 2008) to the observed ones to break the degeneracy inside the box, and accept the best-fit model as a representative model of the concerned star. In this manner, we get an ensemble of approximately 1,000 to 2,000 representative models (depending on the total number of mesh points) for each star. Note that the number of models in the ensemble is not exactly same as the number of mesh points, because not all the tracks enter the box.

We took two different approaches to get the best-fit model from the above ensemble: the first approach used the conventional spectroscopic and seismic data but did not use the glitch information (termed as '*SeismicFit1*'), while the second used all the information including from the glitches (termed as '*GlitchFit*'). These two approaches are used only for the MESA models. In *SeismicFit1*, we defined a cost function,

$$\chi^2_{\rm seismic} = \sum_p \left(\frac{p_{\rm mod} - p_{\rm obs}}{\sigma_p}\right)^2, \tag{5}$$

where p represents 6 observable quantities; the $T_{\rm eff}$, [Fe/H], large frequency separation averaged over the radial modes $\langle\Delta\nu\rangle_0$, average two-point frequency ratio $\langle r_{02}\rangle$, and the five-point ratios $r_{01}(n_0)$ and $r_{01}(n_0+3)$ (n_0 is suitably chosen radial order, and the choice of n_0+3 is made to avoid the correlation among the observables). We refer the reader to Roxburgh & Vorontsov (2003) for the definition of the ratios. The $\chi^2_{\rm seismic}$ was minimized over the model ensemble to get the best-fit model, and the uncertainties on the fitted parameters were estimated from the envelope of the $\chi^2_{\rm seismic}$

($\Delta\chi^2_{\rm seismic} = 1$). The detailed results for the LEGACY sample obtained using this approach were already presented in Silva Aguirre et al. (2016, see sections and results relevant to 'V&A'). Here, we only compare some of those results with the results obtained when using the additional information from the glitch analysis (see the next paragraph).

In *GlitchFit*, we incorporated the information coming from the glitch analysis to our fitting pipeline. For this purpose, we fitted the signatures of the acoustic glitches in the frequencies of all the models in the ensemble using Method A to find the various parameters associated with the base of the convection zone and helium ionization zone, and defined a cost function,

$$\chi^2_{\rm glitch} = \chi^2_{\rm seismic} + \sum_q \left(\frac{q_{\rm mod} - q_{\rm obs}}{\sigma_q} \right)^2, \qquad (6)$$

where q represents 3 observable quantities; amplitude of helium signature averaged over the frequency range $A_{\rm He}$, width of the Γ_1-peak $\Delta_{\rm He} = \sqrt{c_2/8\pi^2}$ (Houdek & Gough 2007), and the acoustic depth of the Γ_1-peak. Note that there is no ambiguity in comparing the acoustic depths of the helium ionization zone as obtained by fitting the observed and model frequencies. A model representing the star must have similar helium glitch as the star, and should leave similar signature on the oscillation frequencies, and hence the fitted $\tau_{\rm He}$ for both must be close. The differences arise when we try to associate the fitted acoustic depth to a layer in the helium ionization zone (see, e.g., Broomhall et al. 2014; Verma et al. 2014a). We did not include the parameters associated with the CZ signature in the definition of $\chi^2_{\rm glitch}$ for the reasons that we discussed earlier in Section 3.1. We minimized the $\chi^2_{\rm glitch}$ over the ensemble to get the best-fit model, and the uncertainties on the fitted parameters were estimated in the same way as in *SeismicFit1*. The MESA model in the subsequent sections would always refer to the best-fit model obtained in this manner, unless stated otherwise.

The above methods find the best-fit model in two steps. In the first step, we fix the evolutionary stage for a set of initial conditions (M, Y_i, [Fe/H]$_i$, $\alpha_{\rm MLT}$, $\alpha_{\rm OV}$) using oscillation frequencies, and filter out reasonable models of the star. The oscillation frequencies monotonically decrease as a star evolves, and hence reasonably constrain the evolutionary stage for a given initial condition. The model frequencies have systematic uncertainties due to the surface effect, hence we do not use them in the second step, instead use the quantities that are relatively insensitive to the surface effect, viz., the frequency ratios. In this manner, we use both the oscillation frequencies and their combinations to get the best-fit model. Since the methods preserve a set of reasonable models of the star, we may plot chi-square as a function of different stellar parameters, which gives additional useful information, e.g., the possibility of the secondary solutions.

4.2. *YREC models*

A second set of best-fit models were calculated using the Yale Rotating Stellar Evolution Code (YREC; Demarque et al. 2008). The models used OPAL high temperature opacities (Iglesias & Rogers 1996) supplemented with low-temperature opacities of Ferguson et al. (2005). We used the 2005 version of the OPAL equation of state (Rogers & Nayfonov 2002). All nuclear reaction rates were from Adelberger et al. (1998) except for $^{14}{\rm N}(p,\gamma)^{15}O$ reaction, for which we used the updated rates of Formicola et al. (2004). A large subset of the models included the diffusion of helium and other heavy elements with the diffusion coefficients from Thoul et al. (1994). The coefficients, however, were changed with a multiplicative factor that depended on the mass of the models to inhibit the complete depletion of helium and heavy elements in the envelope convection zone. The coefficients were unchanged for the models with masses up to of 1.25 $M_\odot$, while for higher masses the coefficients were multiplied by a factor, $f = \exp\left[-\frac{(M-1.25)^2}{2(0.085)^2}\right]$, where M is the mass in solar unit.

The Yale Monte-Carlo Method (YMCM; Silva Aguirre et al. 2015) was used to determine the best-fit model ('*SeismicFit2*'). This fitting method also does not use the glitch information and have been applied only to the YREC models. The reason for using two different names (*SeismicFit1* and *SeismicFit2*) is that the detailed optimization process and the observables used are different in the two cases. For each star, we start with using the average large frequency separation and frequency of maximum power along with the spectroscopic estimate of the effective temperature to get an estimate of the mass (M) and radius (R) of the star using the Yale Birmingham Grid-Based modeling pipeline (Basu et al. 2010; Gai et al. 2011). Since each of the observables has an associated error, we created several realizations of M, R, $T_{\rm eff}$, and [Fe/H]. For each realization (M, R, $T_{\rm eff}$, [Fe/H]), we used YREC in an iterative mode to obtain a model of the given mass M and [Fe/H] that had the required R and $T_{\rm eff}$. This was done in two different ways: in the first approach, we kept $\alpha_{\rm MLT}$ fixed at different values and iterated over Y_i to get the model; and in the second approach, we kept Y_i fixed at different values and varied $\alpha_{\rm MLT}$ to get the required model.

We computed the oscillation frequencies for all the models, and defined a cost function,

$$\chi^2_{\rm total} = \chi^2_\nu + \chi^2_{\rm ratios} + \chi^2_{T_{\rm eff}} + \chi^2_{\rm [Fe/H]}, \qquad (7)$$

where χ^2_ν was calculated using the surface corrected model frequencies (two term formulation of Ball & Gizon 2014), while $\chi^2_{\rm ratios}$ was obtained using the uncorrected model frequencies (contains terms corresponding to both, r_{02} and r_{01}). The first two terms on the right hand side are reduced chi-squares. Since the ratios are strongly correlated, the full error covariance matrix was used to define $\chi^2_{\rm ratios}$. The best-fit model for a star was the one with the lowest value of $\chi^2_{\rm total}$.

5. RESULTS

We fitted the signatures of the acoustic glitches in the oscillation frequencies of all the 66 stars using both methods described in Section 3. The quality of fit primarily depends on the mass of star. Figures 2 and 3 show respectively the fits obtained using Methods A and B for KIC 8760414, 6116048, and 10068307. These stars with masses close to 0.80, 1.05, and 1.36 $M_\odot$, respectively, were selected to be representative of sub-solar, near-solar,

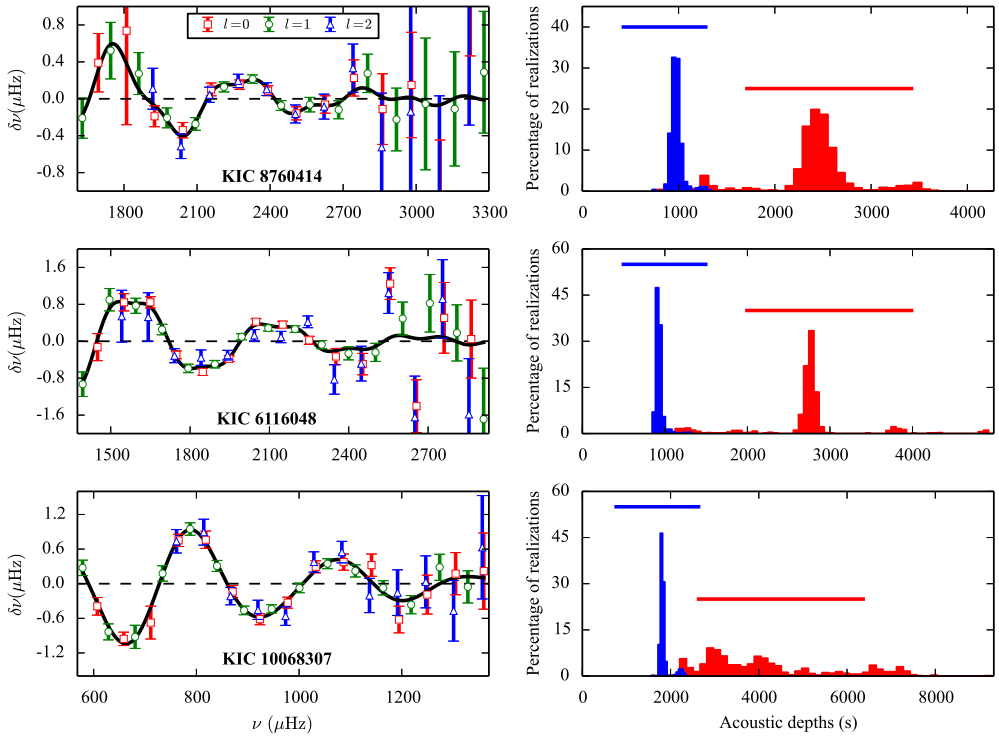

FIG. 2.— Fits to the observed oscillation frequencies of three stars using Method A. The left panels show the oscillatory part of the frequency, $\delta\nu$, obtained by subtracting the smooth part, P_l, from them. The different points represent the observed frequencies, and the continuous line shows the best-fit to them. The right panels show the distribution of the acoustic depths of the CZ glitch (red histogram) and the He glitch (blue histogram). The horizontal bars show the ranges of initial guesses used for these two fitting parameters to search for the global minimum.

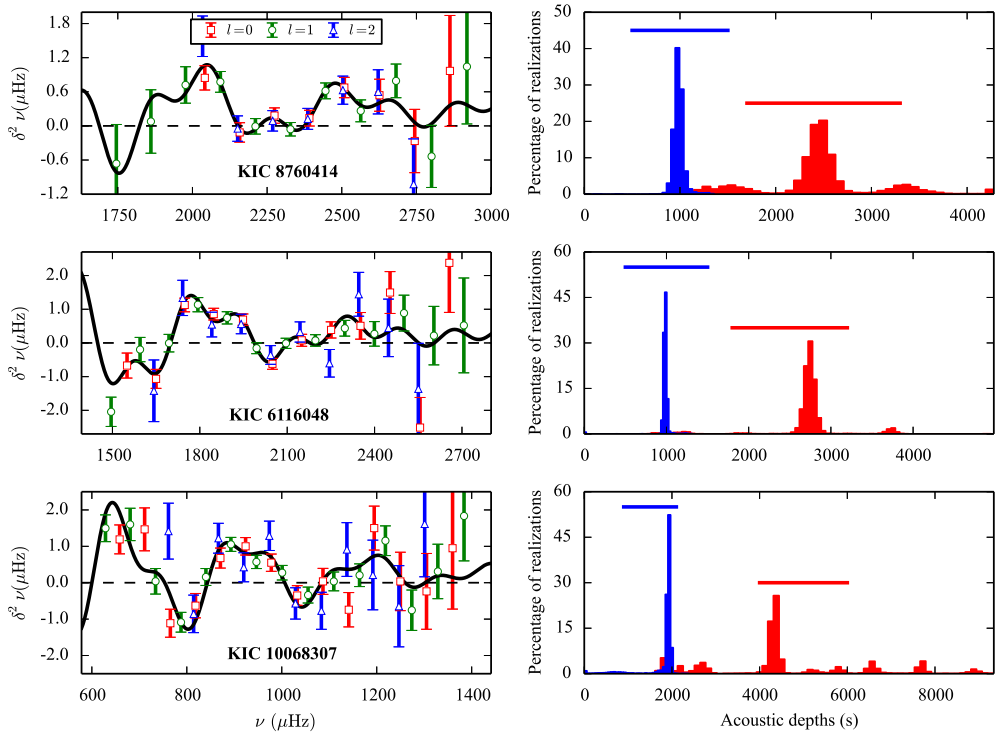

FIG. 3.— Fits to the second differences of the observed oscillation frequencies using Method B. The different points in the left panels represent the observed second differences, and the continuous line shows the best-fit to them. The right panels show the distribution of the acoustic depths of the CZ glitch (red histogram) and the He glitch (blue histogram). The horizontal bars show the ranges of initial guesses used for these two fitting parameters to search for the global minimum.

and super-solar mass stars. Note the small amplitude of the helium signature in the fit for KIC 8760414. This is expected for the low-mass stars because the depression in their Γ_1-profile in the second helium ionization zone is shallow (see, e.g., Verma et al. 2014a), hence the amplitude of the peak between the He I and He II ionization zones is small, consequently the amplitude of the helium signature is small. For low-mass stars, the small amplitude makes it difficult to fit the He signature unless sufficiently low radial order modes are observed. We found that the fit to the He signature was robust for all stars in the LEGACY sample, giving rise to a sharply peaked unimodal distribution of $\tau_{\rm He}$ (see, Figures 2 and 3). The fit to the CZ signature was also generally robust for stars of sub-solar and solar masses, with only a few problematic cases. However, fitting CZ signature was difficult for super-solar mass stars, particularly for stars of $M > 1.20$ M$_\odot$, which gave rise to multiple peaks in the distribution of $\tau_{\rm CZ}$. Such stars are generally hot, and the envelope convection excites modes with shorter life-time, which leads to larger line-width of the modes and larger errorbar on the mode frequencies. For some problematic stars, most of the oscillation frequencies have errorbars that are larger than the average amplitude of the CZ signature.

We modeled each star in the LEGACY sample using the approaches described in Section 4 to find the best-fit model and corresponding oscillation frequencies. Recall that the approach *GlitchFit* involves fitting the signatures of the acoustic glitches in the model frequencies using Method A. We used the same set of modes for the models as used for the observations. Table 1 lists the acoustic depths of the CZ and He glitch and average amplitude of the He glitch for both the observed frequencies and best-fit model frequencies from *GlitchFit*, as well as the mass, radius, and the age for all stars.

For the sake of a clear presentation, we show here that the results obtained using Methods A and B agree very well, and then present the results obtained using only Method A in most of the subsequent sections. Figure 4 shows the differences between the acoustic depths obtained using Methods A and B. We can see an excellent level of agreement between the results of the two methods. This, however, does not guarantee the accuracy of the results. In fact, the acoustic depth of the base of the convection zone is incorrect for some stars in the sample. In such cases, both methods give systematically incorrect $\tau_{\rm CZ}$, as also noted by Reese et al. (2016).

5.1. *Acoustic depths of the CZ and He glitches*

The glitches observed in Sun-like main-sequence stars are regions of only sharp variation in sound speed (not discontinuities in sound speed), and are extended in depth, particularly the glitch arising from the helium ionization zone. To compare the acoustic depths obtained using glitch analysis with the acoustic depth of the layer which causes the signature, we computed the acoustic depths of layers using sound-speed profile of the best-fit model,

$$\tau_r = \int_r^{R_*} \frac{dr}{c}, \tag{8}$$

where r is the radial distance of the layer, R_* the radius of the star (to the acoustic surface and not to the photosphere), and c is the sound speed.

The top panel of Figure 5 compares the different estimates of the acoustic depth of the base of the convection zone. The acoustic depth obtained by fitting the best-fit model frequencies agrees quite well with the acoustic depth calculated using the corresponding sound-speed profile. The calculation of the acoustic depth using sound-speed profile requires the definition of the acoustic surface, which is uncertain. Balmforth & Gough (1990) have argued that the acoustic surface of a star should be defined at a radial distance in the atmosphere where the extrapolated c^2 from the outer convection zone vanishes (see also, Lopes & Gough 2001). An uncertainty in the definition of the acoustic surface introduces a fixed shift in the acoustic depths calculated using sound-speed profile. Here, we assumed the acoustic surface to be the top most layer of the Eddington atmosphere ($\tau = 10^{-5}$). The scaled differences of less than 0.03 between the fitted and calculated acoustic depths suggest that the true acoustic surface is not very far from the assumed layer. The points corresponding to the difference between the acoustic depths obtained by fitting the observed and best-fit model frequencies are more scattered. This is primarily due to the fact that the observed frequencies have associated observational uncertainties, and the fit to the weak CZ signature in the observed frequencies is more prone to aliasing than the fit to the model frequencies.

The helium ionization zones are extended in depth. Traditionally, it has been assumed while modeling the form of the He glitch signature that it arises from the He II ionization zone (see, e.g., Monteiro & Thompson 1998; Houdek & Gough 2007), which implies that the fitted acoustic depth should represent a layer in the He II ionization zone where Γ_1 is minimum ('dip'). Recently, Broomhall et al. (2014) and Verma et al. (2014a) found respectively in the red-giant and main-sequence stellar models that the fitted acoustic depth corresponds more closely to a layer between the He I and He II ionization zones where Γ_1 is maximum ('peak'). The bottom panel of Figure 5 compares the different estimates of the acoustic depth of the helium ionization zone. The acoustic depths obtained by fitting the observed and best-fit model frequencies are in good agreement, as expected. We confirm that the fitted acoustic depth matches with the acoustic depth of the peak in Γ_1-profile.

5.2. *Ensemble study*

Figure 6 shows the acoustic depths of the CZ and He glitch for all the 66 stars in the sample. The results obtained using the two methods look very similar, except that the errorbars obtained using Method B is on average larger than Method A, particularly the errorbar on the acoustic depth of the helium ionization zone. This may be expected because the errorbars on the second differences increase by about a factor 2.5 in comparison to the errorbars on the oscillation frequencies, while the amplitude of the signature increases approximately by a factor $4\sin^2(2\pi\tau_{\rm g}\langle\Delta\nu\rangle)$ (Basu et al. 1994). The factor $4\sin^2(2\pi\tau_{\rm g}\langle\Delta\nu\rangle)$ is generally smaller than 2.5 for the He signature (≈ 1.8, 1.2, and 1.3 for KIC 8760414, 6116048, and 10068307, respectively), effectively reducing its significance in the second differences in comparison to the frequencies. There is a clear correlation seen in Figure 6

TABLE 1
PHYSICAL PARAMETERS FOR ALL STARS IN THE *Kepler* SEISMIC LEGACY SAMPLE.

KIC	Glitch parameters using Method A						Stellar parameters using *GlitchFit*		
	$\tau_{\rm CZ,obs}$ (s)	$\tau_{\rm CZ,mod}$ (s)	$A_{\rm He,obs}$ (μHz)	$A_{\rm He,mod}$ (μHz)	$\tau_{\rm He,obs}$ (s)	$\tau_{\rm He,mod}$ (s)	M ($M_\odot$)	R ($R_\odot$)	t (Gyr)
1435467[a]	5307^{+80}_{-91}	2898	$1.067^{+0.076}_{-0.072}$	0.957	1112^{+37}_{-35}	1056	1.39 ± 0.04	1.706 ± 0.020	2.7 ± 0.3
2837475[a]	2422^{+65}_{-65}	1884	$1.895^{+0.144}_{-0.145}$	1.609	905^{+26}_{-27}	843	1.50 ± 0.04	1.659 ± 0.020	1.7 ± 0.2
3427720	2068^{+99}_{-78}	2289	$0.590^{+0.079}_{-0.075}$	0.633	817^{+56}_{-47}	668	1.15 ± 0.03	1.130 ± 0.015	2.4 ± 0.2
3456181[b]	5259^{+341}_{-504}	4373	$1.088^{+0.073}_{-0.122}$	0.689	1689^{+56}_{-62}	1657	1.50 ± 0.04	2.157 ± 0.020	2.6 ± 0.3
3632418	4149^{+188}_{-153}	4157	$0.727^{+0.030}_{-0.034}$	0.655	1498^{+35}_{-35}	1420	1.31 ± 0.04	1.867 ± 0.020	2.8 ± 0.3
3656476	3710^{+107}_{-126}	3575	$0.536^{+0.075}_{-0.055}$	0.435	961^{+41}_{-32}	993	1.09 ± 0.03	1.322 ± 0.015	8.4 ± 0.4
3735871	1988^{+77}_{-75}	2323	$0.598^{+0.084}_{-0.071}$	0.589	845^{+60}_{-70}	651	1.20 ± 0.04	1.133 ± 0.020	1.5 ± 0.2
4914923	3444^{+258}_{-168}	3497	$0.580^{+0.032}_{-0.033}$	0.553	1060^{+32}_{-32}	1025	1.07 ± 0.03	1.357 ± 0.015	6.8 ± 0.3
5184732	2810^{+70}_{-95}	3117	$0.735^{+0.086}_{-0.085}$	0.663	849^{+38}_{-32}	826	1.17 ± 0.03	1.329 ± 0.015	4.0 ± 0.4
5773345	3352^{+189}_{-143}	4099	$0.798^{+0.060}_{-0.065}$	0.785	1505^{+38}_{-32}	1491	1.55 ± 0.04	2.045 ± 0.020	2.5 ± 0.4
5950854	3827^{+191}_{-234}	3275	$0.410^{+0.170}_{-0.098}$	0.236	1681^{+164}_{-200}	1062	1.03 ± 0.02	1.269 ± 0.010	10.3 ± 0.4
6106415	2707^{+109}_{-111}	2685	$0.542^{+0.036}_{-0.033}$	0.522	861^{+30}_{-30}	832	1.05 ± 0.04	1.209 ± 0.020	4.9 ± 0.3
6116048	2761^{+54}_{-60}	2790	$0.467^{+0.028}_{-0.027}$	0.448	922^{+25}_{-23}	893	1.05 ± 0.02	1.235 ± 0.010	5.7 ± 0.3
6225718	2207^{+328}_{-168}	2425	$0.910^{+0.042}_{-0.041}$	0.919	773^{+15}_{-14}	736	1.12 ± 0.03	1.220 ± 0.015	2.5 ± 0.2
6508366[a]	3325^{+130}_{-161}	4688	$0.936^{+0.080}_{-0.077}$	0.904	1527^{+61}_{-58}	1495	1.37 ± 0.04	2.105 ± 0.020	2.3 ± 0.2
6603624	3089^{+77}_{-68}	2976	$0.370^{+0.023}_{-0.023}$	0.389	875^{+26}_{-28}	818	1.05 ± 0.02	1.167 ± 0.010	8.1 ± 0.3
6679371	3913^{+182}_{-163}	2937	$1.278^{+0.094}_{-0.103}$	1.200	1375^{+48}_{-54}	1352	1.63 ± 0.04	2.248 ± 0.020	2.0 ± 0.3
6933899	4395^{+297}_{-206}	4179	$0.466^{+0.021}_{-0.024}$	0.401	1499^{+41}_{-42}	1374	1.12 ± 0.03	1.583 ± 0.015	6.6 ± 0.4
7103006[a]	2941^{+268}_{-190}	3804	$0.876^{+0.100}_{-0.088}$	0.644	1292^{+70}_{-77}	1407	1.35 ± 0.04	1.903 ± 0.020	2.4 ± 0.3
7106245	2916^{+175}_{-234}	2236	$0.542^{+0.181}_{-0.120}$	0.397	835^{+115}_{-121}	793	0.93 ± 0.02	1.100 ± 0.010	7.1 ± 0.3
7206837	2665^{+194}_{-107}	3097	$1.113^{+0.121}_{-0.115}$	0.894	976^{+43}_{-40}	985	1.36 ± 0.04	1.588 ± 0.020	3.1 ± 0.4
7296438	3635^{+210}_{-206}	3630	$0.488^{+0.068}_{-0.067}$	0.463	1098^{+78}_{-81}	986	1.15 ± 0.03	1.393 ± 0.015	6.6 ± 0.3
7510397[a]	4982^{+155}_{-157}	3999	$0.602^{+0.028}_{-0.025}$	0.535	1606^{+34}_{-39}	1469	1.27 ± 0.04	1.821 ± 0.020	3.3 ± 0.3
7680114[a]	2697^{+304}_{-257}	3739	$0.435^{+0.069}_{-0.041}$	0.527	1205^{+61}_{-66}	1082	1.13 ± 0.03	1.423 ± 0.015	7.2 ± 0.3
7771282	3792^{+229}_{-231}	3684	$0.893^{+0.137}_{-0.125}$	0.776	1375^{+104}_{-113}	1051	1.30 ± 0.03	1.659 ± 0.015	2.9 ± 0.3
7871531	2117^{+74}_{-59}	2091	$0.237^{+0.035}_{-0.049}$	0.163	749^{+59}_{-84}	629	0.80 ± 0.02	0.858 ± 0.010	9.2 ± 0.4
7940546	3673^{+95}_{-93}	4368	$0.754^{+0.037}_{-0.041}$	0.651	1551^{+37}_{-38}	1463	1.33 ± 0.03	1.915 ± 0.015	2.7 ± 0.3
7970740	1955^{+65}_{-79}	1824	$0.215^{+0.045}_{-0.041}$	0.198	551^{+38}_{-48}	580	0.73 ± 0.03	0.761 ± 0.015	10.1 ± 0.4
8006161	2264^{+92}_{-83}	2163	$0.424^{+0.053}_{-0.045}$	0.457	563^{+20}_{-20}	552	1.00 ± 0.03	0.933 ± 0.015	4.9 ± 0.2
8150065[a]	3749^{+154}_{-157}	2779	$0.707^{+0.506}_{-0.707}$	0.629	1012^{+371}_{-358}	854	1.12 ± 0.03	1.367 ± 0.015	4.0 ± 0.3
8179536	2363^{+61}_{-55}	2308	$1.076^{+0.115}_{-0.110}$	1.000	803^{+55}_{-55}	757	1.20 ± 0.03	1.331 ± 0.015	1.6 ± 0.2
8228742	4521^{+93}_{-94}	4736	$0.545^{+0.031}_{-0.028}$	0.509	1578^{+38}_{-38}	1491	1.28 ± 0.03	1.825 ± 0.015	4.6 ± 0.4
8379927	2219^{+222}_{-209}	2160	$0.704^{+0.029}_{-0.033}$	0.654	703^{+21}_{-22}	659	1.11 ± 0.03	1.114 ± 0.015	1.7 ± 0.2
8394589[b]	1952^{+108}_{-148}	2373	$0.793^{+0.065}_{-0.058}$	0.683	750^{+50}_{-44}	769	1.08 ± 0.04	1.178 ± 0.020	3.9 ± 0.3
8424992	2662^{+312}_{-256}	2636	$0.412^{+0.178}_{-0.116}$	0.179	1045^{+155}_{-210}	766	0.95 ± 0.03	1.060 ± 0.015	9.1 ± 0.3
8694723	3281^{+69}_{-60}	3793	$0.693^{+0.035}_{-0.038}$	0.678	1245^{+31}_{-30}	1220	1.09 ± 0.03	1.522 ± 0.015	4.5 ± 0.3
8760414	2455^{+131}_{-127}	2528	$0.222^{+0.029}_{-0.026}$	0.181	968^{+36}_{-37}	929	0.80 ± 0.02	1.018 ± 0.010	12.4 ± 0.4
8938364	4044^{+66}_{-69}	3891	$0.390^{+0.024}_{-0.023}$	0.343	1243^{+45}_{-39}	1170	1.06 ± 0.03	1.386 ± 0.015	9.8 ± 0.4
9025370[b]	1722^{+108}_{-105}	2321	$0.322^{+0.103}_{-0.055}$	0.244	810^{+137}_{-144}	643	1.02 ± 0.03	1.021 ± 0.015	5.0 ± 0.3
9098294	3128^{+133}_{-213}	2833	$0.449^{+0.041}_{-0.046}$	0.343	837^{+30}_{-26}	856	0.97 ± 0.02	1.145 ± 0.010	8.0 ± 0.3
9139151[a]	3239^{+88}_{-79}	2277	$0.683^{+0.063}_{-0.062}$	0.698	788^{+30}_{-33}	685	1.20 ± 0.03	1.168 ± 0.015	1.9 ± 0.2
9139163[a]	2182^{+44}_{-51}	2318	$1.335^{+0.073}_{-0.067}$	1.138	865^{+22}_{-22}	889	1.34 ± 0.04	1.542 ± 0.020	2.2 ± 0.3
9206432	2839^{+64}_{-62}	2351	$1.489^{+0.117}_{-0.100}$	1.005	892^{+39}_{-34}	845	1.38 ± 0.04	1.513 ± 0.020	2.0 ± 0.3
9353712[b]	6305^{+154}_{-165}	4028	$0.775^{+0.103}_{-0.097}$	0.766	1612^{+71}_{-69}	1599	1.53 ± 0.04	2.178 ± 0.020	2.7 ± 0.3
9410862	2760^{+125}_{-106}	2692	$0.430^{+0.055}_{-0.077}$	0.374	1065^{+58}_{-53}	838	1.03 ± 0.03	1.178 ± 0.015	6.4 ± 0.3
9414417	4289^{+157}_{-199}	4665	$0.768^{+0.058}_{-0.055}$	0.694	1468^{+41}_{-38}	1396	1.29 ± 0.03	1.865 ± 0.015	3.5 ± 0.3
9812850[b]	4671^{+363}_{-196}	4368	$1.154^{+0.097}_{-0.103}$	0.782	1291^{+44}_{-41}	1297	1.26 ± 0.04	1.760 ± 0.020	3.3 ± 0.3
9955598	1940^{+115}_{-417}	2089	$0.250^{+0.627}_{-0.115}$	0.195	980^{+360}_{-572}	548	0.87 ± 0.02	0.877 ± 0.010	6.5 ± 0.3
9965715[b]	2800^{+270}_{-150}	2318	$0.907^{+0.111}_{-0.091}$	0.843	825^{+45}_{-53}	738	1.07 ± 0.04	1.269 ± 0.020	3.2 ± 0.3
10068307[b]	4000^{+298}_{-318}	5349	$0.601^{+0.031}_{-0.036}$	0.508	1813^{+27}_{-31}	1719	1.36 ± 0.03	2.053 ± 0.015	3.2 ± 0.4
10079226	2960^{+101}_{-372}	2460	$0.518^{+0.109}_{-0.088}$	0.494	870^{+105}_{-129}	678	1.11 ± 0.03	1.145 ± 0.015	2.8 ± 0.2
10162436	4316^{+211}_{-253}	4024	$0.775^{+0.037}_{-0.040}$	0.767	1579^{+39}_{-37}	1499	1.18 ± 0.04	1.898 ± 0.020	3.7 ± 0.3
10454113	2189^{+74}_{-94}	2362	$1.079^{+0.071}_{-0.075}$	0.942	734^{+19}_{-22}	722	1.16 ± 0.03	1.237 ± 0.015	1.9 ± 0.2
10516096	3646^{+120}_{-102}	3602	$0.484^{+0.034}_{-0.036}$	0.432	1167^{+41}_{-42}	1112	1.17 ± 0.03	1.447 ± 0.015	6.2 ± 0.3
10644253[b]	1804^{+65}_{-82}	2229	$0.866^{+0.103}_{-0.091}$	0.907	675^{+36}_{-42}	616	1.12 ± 0.03	1.105 ± 0.015	1.1 ± 0.1
10730618	3691^{+100}_{-89}	3947	$1.207^{+0.132}_{-0.138}$	0.701	1260^{+54}_{-47}	1235	1.23 ± 0.04	1.729 ± 0.020	3.1 ± 0.3
10963065	2900^{+180}_{-190}	2716	$0.659^{+0.065}_{-0.055}$	0.646	793^{+47}_{-40}	826	1.08 ± 0.03	1.228 ± 0.015	4.1 ± 0.3
11081729	2339^{+206}_{-325}	2802	$1.022^{+0.155}_{-0.139}$	0.994	923^{+99}_{-121}	740	1.25 ± 0.04	1.416 ± 0.020	2.2 ± 0.3
11253226	1954^{+95}_{-73}	2018	$2.016^{+0.105}_{-0.119}$	1.965	843^{+23}_{-22}	774	1.43 ± 0.04	1.610 ± 0.020	1.9 ± 0.3
11772920	1847^{+368}_{-170}	2042	$0.337^{+0.131}_{-0.091}$	0.152	524^{+83}_{-92}	573	0.78 ± 0.03	0.829 ± 0.015	9.5 ± 0.5
12009504	2996^{+94}_{-108}	2992	$0.722^{+0.058}_{-0.058}$	0.687	938^{+50}_{-36}	885	1.14 ± 0.03	1.391 ± 0.015	3.6 ± 0.3
12069127[a]	3902^{+108}_{-113}	4661	$0.863^{+0.094}_{-0.128}$	0.733	1745^{+113}_{-107}	1697	1.61 ± 0.06	2.314 ± 0.030	2.5 ± 0.3
12069424	2839^{+73}_{-73}	3063	$0.451^{+0.044}_{-0.037}$	0.418	910^{+31}_{-32}	886	1.10 ± 0.02	1.237 ± 0.010	6.7 ± 0.3
12069449[b]	1790^{+55}_{-60}	2724	$0.480^{+0.023}_{-0.023}$	0.457	767^{+20}_{-17}	768	1.00 ± 0.03	1.102 ± 0.015	6.9 ± 0.3
12258514	3906^{+218}_{-163}	3864	$0.548^{+0.018}_{-0.021}$	0.526	1274^{+23}_{-20}	1195	1.22 ± 0.03	1.586 ± 0.015	4.3 ± 0.3
12317678[a]	2545^{+68}_{-72}	3991	$1.498^{+0.089}_{-0.083}$	1.035	1115^{+32}_{-30}	1260	1.19 ± 0.04	1.758 ± 0.020	3.4 ± 0.3

NOTE. — The symbols in the header have usual meaning. The quantities with subscript 'obs' are obtained by fitting the observed frequencies, while with 'mod' are found by fitting the best-fit model frequencies from *GlitchFit*.

[a] The distribution of $\tau_{\rm CZ}$ have multiple peaks. There is a small peak close to the $\tau_{\rm CZ}$ obtained using sound-speed profile of the best-fit model, but the acoustic depth corresponding to the dominant peak and its complement are far from the $\tau_{\rm CZ}$. This may happen if the signature is not significant, i.e., the oscillation frequencies have large errorbars.

[b] The fitted acoustic depth of the base of the convection zone is close to the complement of the $\tau_{\rm CZ}$ obtained using sound-speed profile of the best-fit model.

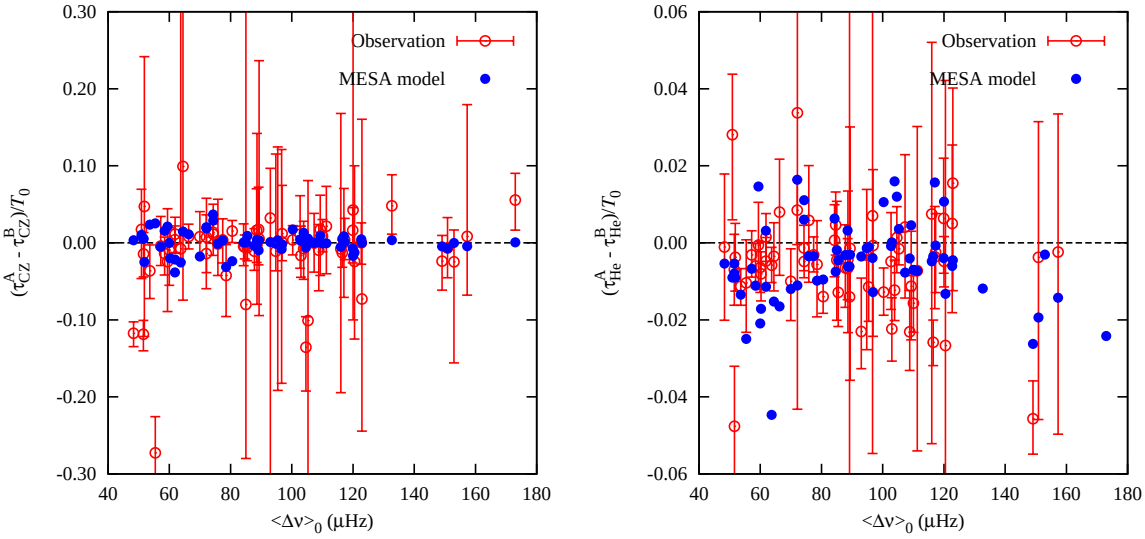

FIG. 4.— Comparison of the acoustic depths (base of the convection zone in the left panel and helium ionization zone in the right panel) obtained using Methods A and B for all stars in the LEGACY sample. The open circles with errorbar correspond to the fit to the observed frequencies, while filled circles to the fit to the best-fit model frequencies.

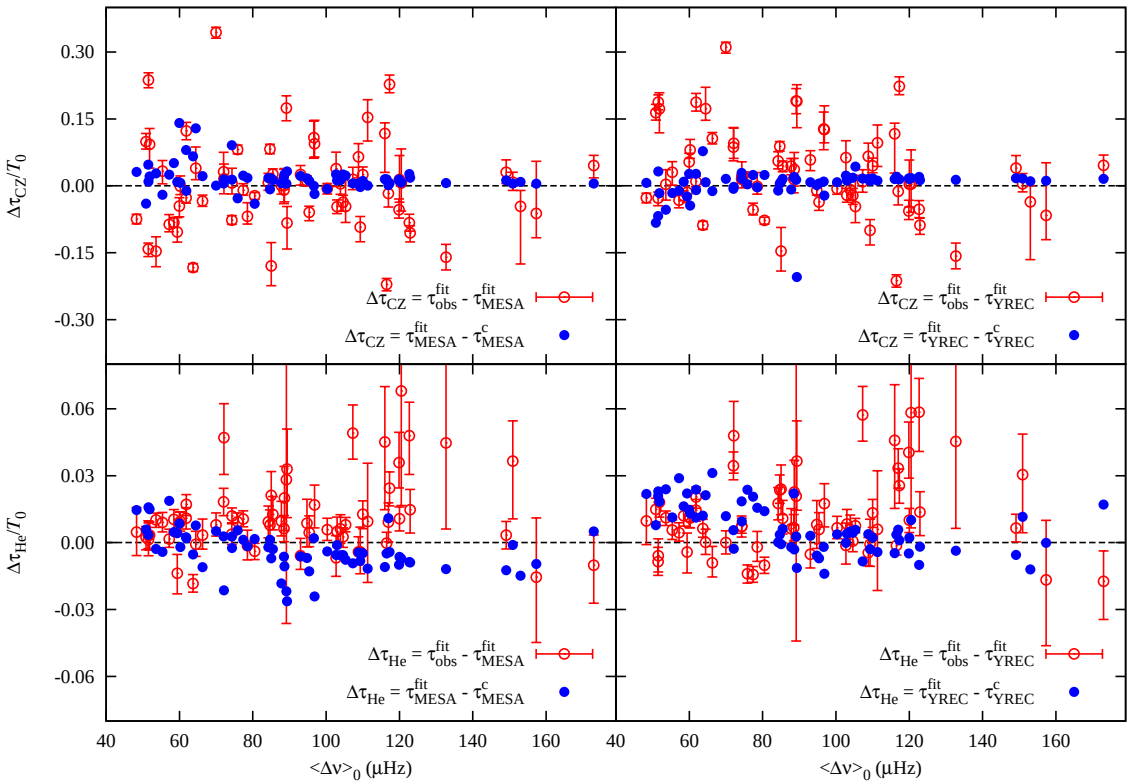

FIG. 5.— Comparison of the acoustic depths obtained using glitch analysis (Method A) and the sound-speed profiles (MESA/YREC). The open circles with errorbar show the scaled difference between the acoustic depths obtained by fitting the observed (τ^{fit}_{obs}) and best-fit model ($\tau^{fit}_{MESA/YREC}$) frequencies, while the blue circles show the scaled difference between the acoustic depths obtained by fitting the best-fit model frequencies and using the sound-speed profile ($\tau^{c}_{MESA/YREC}$). The τ^{c}_{MESA} and τ^{c}_{YREC} in the bottom panels represent the acoustic depth of the peak in first adiabatic index between the He I and He II ionization zones.

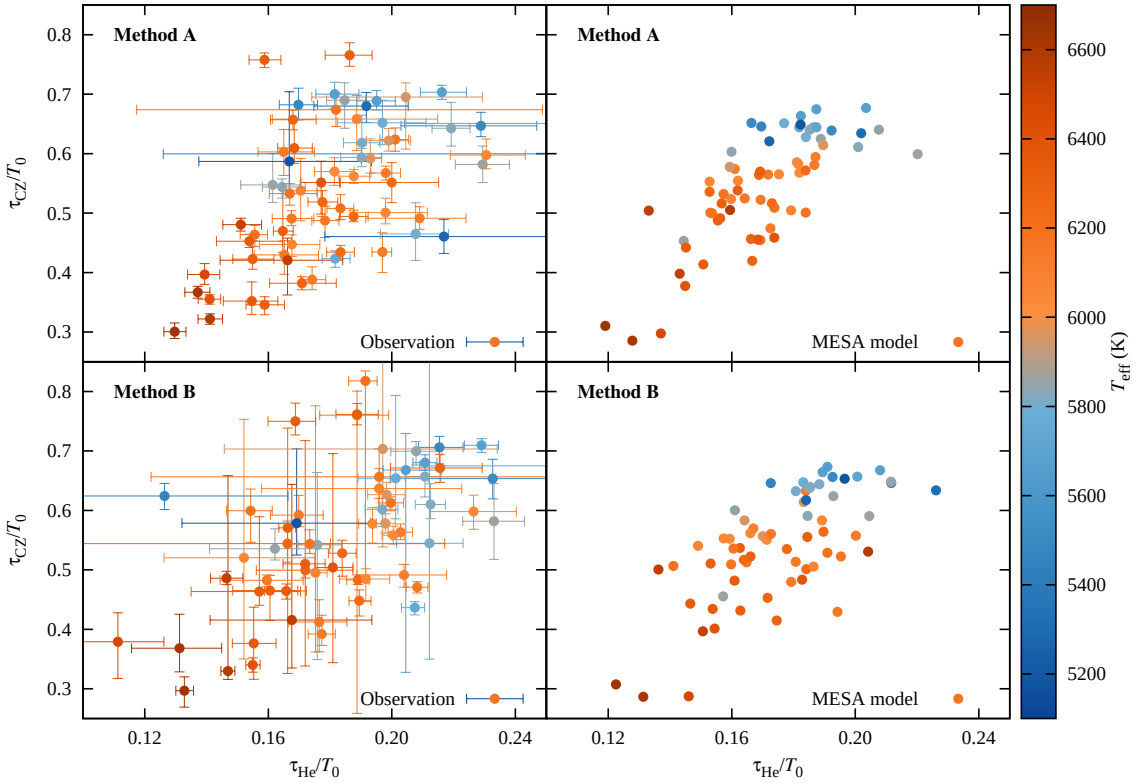

FIG. 6.— Scaled acoustic depths of the base of the convection zone and helium ionization zone as obtained using glitch analysis. A point in a panel represents a star. The points with errorbar in the left panels were obtained by fitting the observed frequencies, while points in the right panels were found by fitting the best-fit model frequencies. The colors represent the effective temperature of the star.

between the acoustic depths of the base of the convection zone and helium ionization zone. The larger scatter seen in the left panels is mostly due to aliasing of the CZ signature. The helium signature is typically strong, and the determination of τ_{He} is reliable. The fitted τ_{He} together with the above correlation may be used to select the correct solution in the cases where the distribution of τ_{CZ} have multiple peaks. As one may expect, the figure also shows that the cooler stars have deeper convection zones as well as deeper helium ionization layers.

Figure 7 shows the scaled acoustic depth of the base of the convection zone obtained using Method A as a function of mass, age, large frequency separation averaged over radial modes, and average two-point ratio. The fit to the model frequencies is not as much affected by the problem of aliasing as the observed frequencies, unveiling the relationships between the acoustic depth of the base of the convection zone and various stellar properties better. The results obtained using Method B look very similar. As can be seen from the topmost panels, the acoustic depth of the base of the convection zone decreases as the mass (hence the effective temperature) increases. This is expected as the hotter stars have smaller opacity, and the radiation can transport the energy in the larger part of the envelope. The acoustic depth of the base of the convection zone increases as a function of the age and average large frequency separation, while it decreases with the two-point ratio. The age and large frequency separation depend on the mass of the star, and the global trend seen in the corresponding panels are result of that dependence. The two-point ratio is an indicator of the evolutionary stage of the star—it decreases as star evolves on the main-sequence—and the dependence seen in the bottom panel can be largely understood in terms of its dependence on the age. The dependence of the τ_{CZ} on composition is significantly weaker than on the mass, and can be seen only if the mass is constrained to a narrow range.

The helium signature in the oscillation frequencies of the Sun-like stars cannot only be used to derive the location of the helium ionization zone but also can be used to estimate the envelope helium abundance. The average amplitude of the helium signature depends on the amount of helium present in its ionization zone (see, e.g., Basu et al. 2004; Monteiro & Thompson 2005; Houdek & Gough 2007), which may be calibrated against the corresponding amplitudes of the helium signatures in the model frequencies of different envelope helium abundance to estimate its abundance (Verma et al. 2014b). Figure 8 shows the acoustic depth of the helium ionization zone as well as the average amplitude of the helium signature as a function of M, t, $\langle\Delta\nu\rangle_0$, and r_{02}. The acoustic depth of the helium ionization zone decreases as the mass increases. This is again expected as the helium gets ionized closer to the surface for hotter stars. The acoustic depth of the helium ionization zone increases as a function of the age and large frequency separation, while it decreases with the two-point ratio. The average amplitude of the helium signature increases with the mass, as was noted by Verma et al. (2014a). This complicates the calibration involved in the helium abundance determination. The amplitude decreases as a

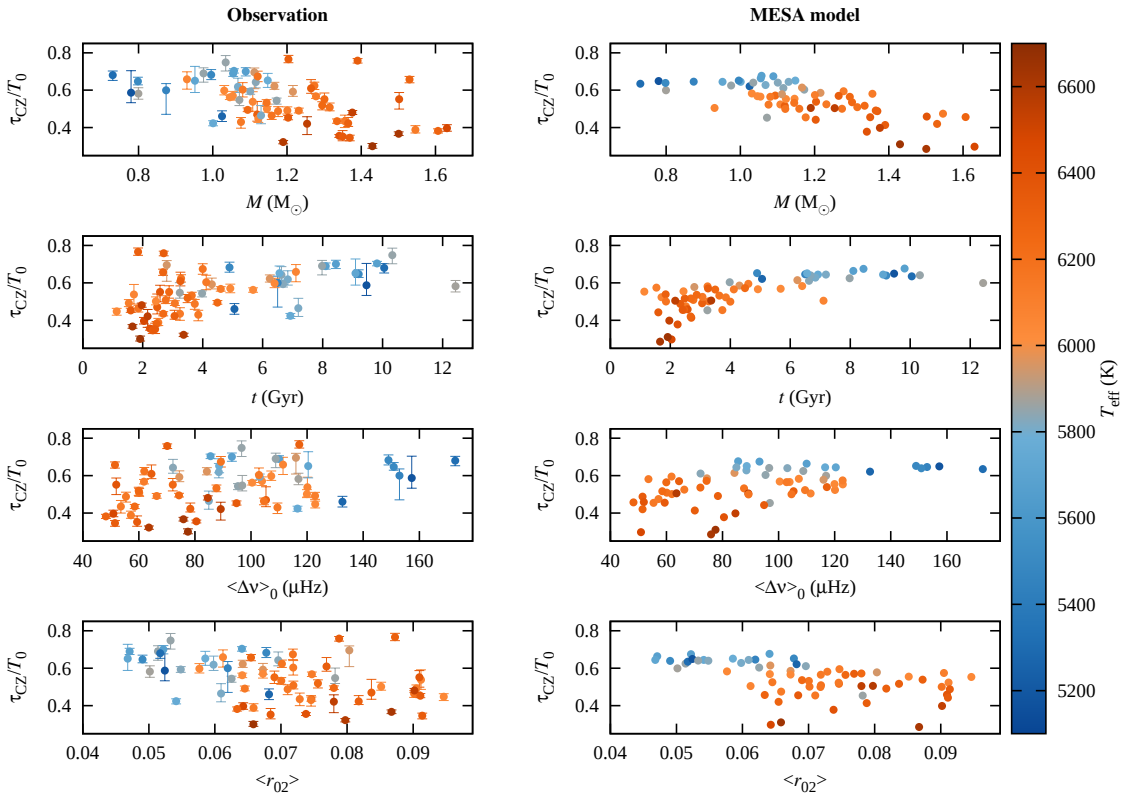

FIG. 7.— Scaled acoustic depth of the base of the convection zone obtained using Method A as a function of different stellar parameters. The points with errorbar in the left panels were obtained by fitting the observed frequencies, while points in the right panels were found by fitting the best-fit model frequencies. The colors represent the effective temperature of the star.

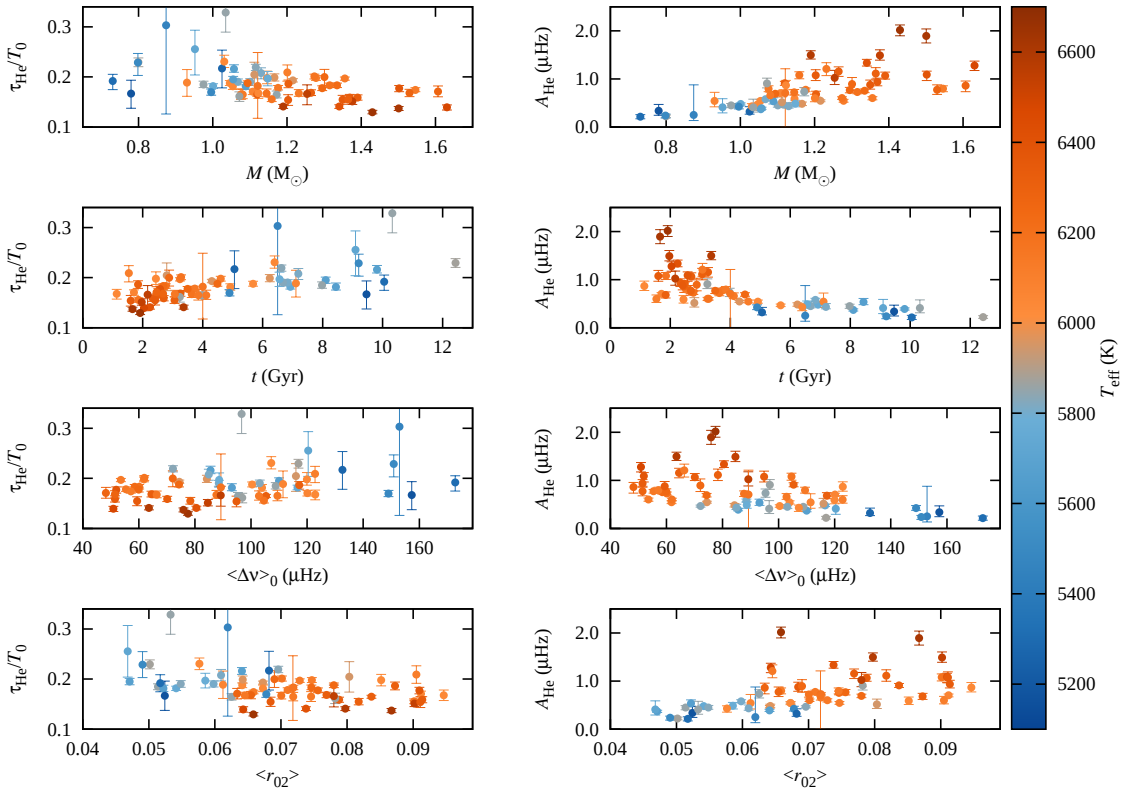

FIG. 8.— Scaled acoustic depth of the helium ionization zone (left panels) and average amplitude of helium signature (right panels) as a function of different stellar parameters. The acoustic depth and the average amplitude were obtained by fitting the observed oscillation frequencies using Method A. The colors represent the effective temperature of the star.

function of the age and large frequency separation, while it increases with the two-point ratio. The variation of the amplitude and the acoustic depth with t, $\langle\Delta\nu\rangle_0$, and r_{02} can again be understood mostly in terms of the variation of these parameters with the mass and effective temperature.

6. THE IMPORTANCE OF ANALYZING ACOUSTIC GLITCHES

The stellar model fitting is a high-dimensional nonlinear optimization problem, and the solution may not always converge to the global minimum. There are several fitting methods in use, e.g., parallel genetic algorithm (Metcalfe et al. 2009), Bayesian approach (Gruberbauer et al. 2012; Silva Aguirre et al. 2015), machine learning method (Verma et al. 2016; Bellinger et al. 2016), etc. The performance of different fitting methods have been compared in the past (see, e.g., Reese et al. 2016; Silva Aguirre et al. 2016). The trouble common to all the methods is that the stellar parameters have intrinsic correlations, e.g., the well known anti-correlation between the mass and initial helium abundance (see, e.g., Metcalfe et al. 2009; Lebreton & Goupil 2014; Verma et al. 2016), and they are not well constrained by the conventional spectroscopic and seismic data, particularly the initial helium abundance.

The best-fit model obtained using only the spectroscopic and seismic data may not accurately reproduce the structure of the star, particularly the helium ionization layers, for the aforementioned reasons. In some cases, the signature of the mismatch of structure of the helium ionization layers in a star and the best-fit model can be seen directly in the difference between the observed and model frequencies. Figure 9 shows the difference between the observed and model frequencies for two such stars. The modulation on top of the surface term for the best-fit models obtained using *SeismicFit1* and *SeismicFit2* is due to the mismatch of the helium signature in the observed and model frequencies. The *GlitchFit* approach fits the glitch parameters and ensures that the observed and best-fit model frequencies have similar helium signature, and consequently have either no modulation or smaller amplitude modulation on top of the surface term. In this section, we illustrate using few individual stars how the glitch analysis helps us constrain the stellar structure better.

6.1. *Sun-as-a-star*

Lund et al. (2016) have also prepared data for the Sun with a noise level similar to the LEGACY sample to assess the results of their peak-bagging, and also to test the results of the modeling done by Silva Aguirre et al. (2016). We modeled the Sun in the same way as stars in the LEGACY sample with and without using the information from the glitch analysis. The first row of Table 2 lists the results obtained without using the information from glitch analysis. The mass and radius were found to be underestimated by about 2σ. The surface helium abundance and the radial distance to the base of the convection zone, as obtained from the best-fit model, were also not consistent with the helioseismic determinations. The chi-square map obtained from the model ensemble suggested the possibility of a secondary solution with mass and radius closer to the solar value, as seen in the left panel of Figure 10.

A closer inspection of the results for the mass and surface helium abundance indicates that the problem could be due to the anti-correlation between the mass and initial helium abundance. A better constraint on the initial helium abundance can help in such situations. The second row of Table 2 lists the results obtained using the supplementary information coming from the glitch analysis. The mass and radius are both now in agreement with the solar mass and radius, and the values for the Y and $R_{\rm CZ}$ are also closer to the helioseismic determinations. The right panel of Figure 10 shows the corresponding chi-square map. Note that the role of the primary and secondary solution has reversed. This is because the primary solution in the left panel corresponds to a model that has significantly larger surface helium abundance than the solar helium abundance, and hence the corresponding oscillation frequencies have larger average amplitude of the helium signature, and contributes significantly to the chi-square if the average amplitude is included in its definition. The secondary solution in the left panel, on the other hand, corresponds to a model that has surface helium abundance similar to the Sun, and hence their oscillation frequencies have similar average amplitude of helium signature, and contributes negligibly to the chi-square if the average amplitude is included in its definition. Figure 11 shows the fit to the observed as well as best-fit model frequencies, and compares their helium signatures. Apart from a small phase shift, the helium signature in the best-fit model frequencies obtained using *GlitchFit* reproduces the observed signature better than the best-fit model frequencies obtained using *SeismicFit1*. Recall that the phase of the helium signature was not included in the definition of $\chi^2_{\rm glitch}$, hence the possibility of a phase difference between the observed and model helium signature is not ruled out. This example clearly demonstrates that how the anti-correlation between the mass and initial helium abundance can lead to problems, and how the glitch analysis can help sort them out.

6.2. *KIC 8760414*

This star is one of the oldest and lowest metallicity star in the LEGACY sample ([Fe/H] $= -0.92 \pm 0.10$). It has been studied previously using *Kepler* data. For instance, Mathur et al. (2012) estimated the mass, radius, age, and the initial helium abundance of the star to be 0.81 ± 0.01 M$_\odot$, 1.02 ± 0.01 R$_\odot$, 13.35 ± 0.38 Gyr, and 0.220 ± 0.018, respectively, while Metcalfe et al. (2014) found them to be 0.78 ± 0.01 M$_\odot$, 1.010 ± 0.004 R$_\odot$, 13.69 ± 0.74 Gyr, and 0.238 ± 0.006. We derived the physical properties of this star without using the information from the glitch analysis, and the results are listed in the third row of Table 2. The small surface helium abundance is a result of both the small initial helium abundance and large helium diffusion. In all the above determinations, the interesting point to note is that the initial helium abundance was found to be significantly sub-primordial ($Y_{\rm P} = 0.2482 \pm 0.0007$; Steigman 2010), and the age to be close to the age of the universe ($t_{\rm U} = 13.799 \pm 0.021$ Gyr; Planck Collaboration et al. 2016).

The fourth row of Table 2 lists the parameters obtained

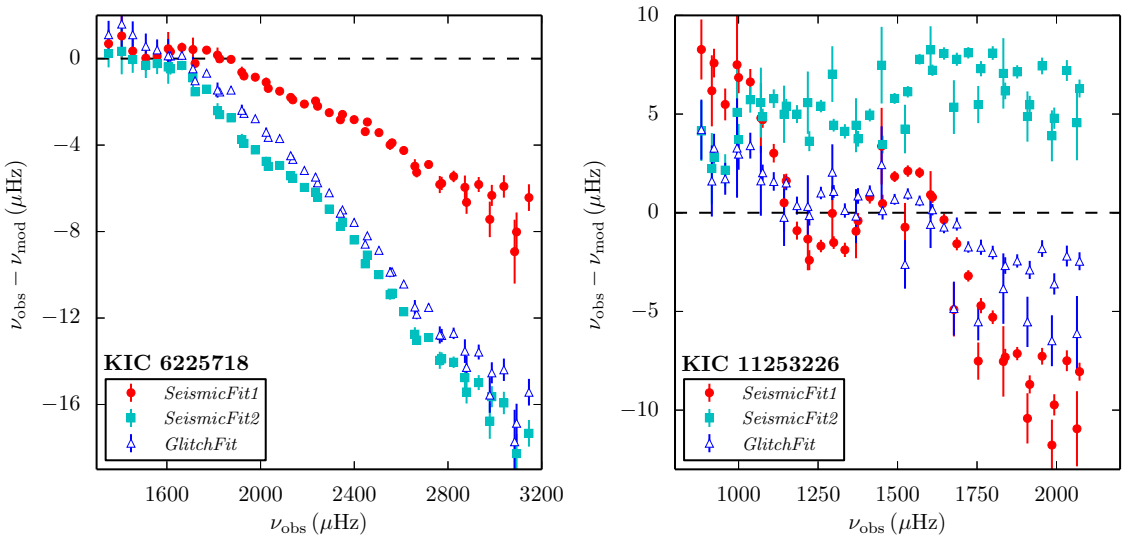

FIG. 9.— Differences between the observed and a set of best-fit uncorrected model frequencies for KIC 6225718 and 11253226. The three different types of points in each panel correspond to three different sets of best-fit model frequencies obtained using methods *SeismicFit1*, *SeismicFit2*, and *GlitchFit*.

TABLE 2
PHYSICAL PARAMETERS OBTAINED WITH AND WITHOUT GLITCH PARAMETERS IN THE STELLAR MODEL FITTING.

Star	Method	M ($M_\odot$)	R ($R_\odot$)	t (Gyr)	L ($L_\odot$)	$\langle\rho\rangle$ (g cm^{-3})	Y	Y_i	R_{CZ} ($R_\odot$)
Sun-as-a-star	*SeismicFit1*	0.93 ± 0.03	0.973 ± 0.015	4.62 ± 0.20	0.937	1.418 ± 0.006	0.277	0.311	0.725
Sun-as-a-star	*GlitchFit*	1.03 ± 0.04	1.013 ± 0.020	4.56 ± 0.30	0.991	1.406 ± 0.007	0.237	0.261	0.717
KIC 8760414	*SeismicFit1*	0.83 ± 0.02	1.029 ± 0.010	13.82 ± 0.40	1.143	1.070 ± 0.003	0.138	0.203	0.773
KIC 8760414	*GlitchFit*	0.80 ± 0.02	1.018 ± 0.010	12.38 ± 0.40	1.136	1.066 ± 0.003	0.183	0.254	0.750
KIC 6106415	*SeismicFit1*	1.05 ± 0.04	1.209 ± 0.020	4.93 ± 0.30	1.699	0.840 ± 0.005	0.221	0.271	0.937
KIC 6106415	*GlitchFit*	1.05 ± 0.04	1.209 ± 0.020	4.93 ± 0.30	1.699	0.840 ± 0.005	0.221	0.271	0.937

NOTE. — The solar helium abundance as obtained using helioseismology is, $Y = 0.248 \pm 0.003$ (Basu 1998), while the radial distance of the base of the solar convection zone is, $R_{CZ} = 0.713 \pm 0.001$ $R_\odot$ (Christensen-Dalsgaard et al. 1991).

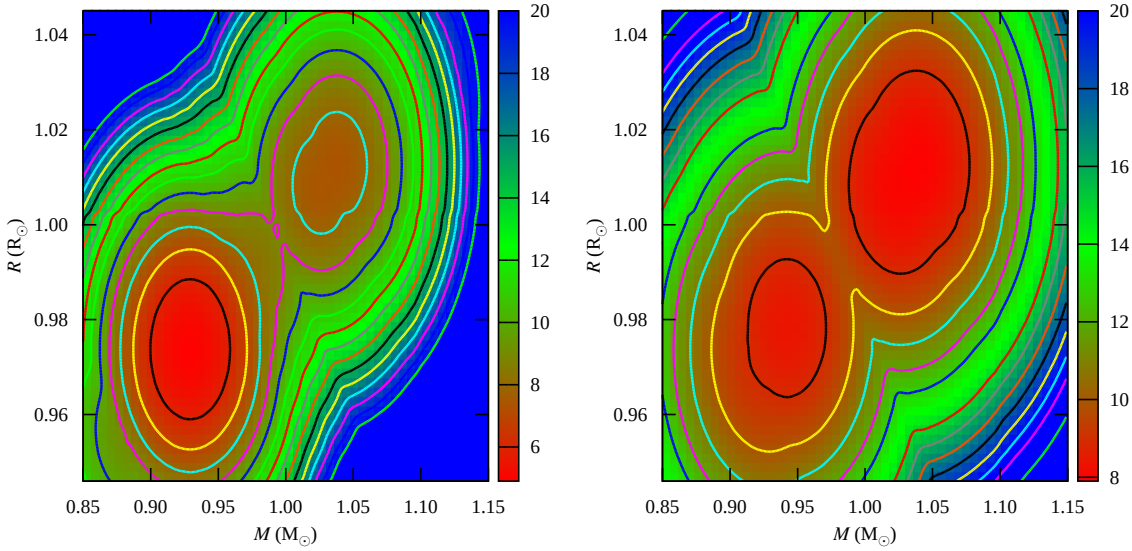

FIG. 10.— Chi-square map as a function of mass and radius obtained from the ensemble of models constructed to fit the Sun-as-a-star data. The chi-square in the left panel includes only the spectroscopic and seismic observables (*SeismicFit1*), while in the right panel it includes additional parameters associated with the helium signature (*GlitchFit*). The contours are uniformly spaced with $\Delta\chi^2 = 1$.

using *GlitchFit*. The initial helium abundance is now greater than the amount of helium produced during the Big Bang nucleosynthesis, and is in line with the expectation from the helium-to-metal enrichment relation. It is interesting to note that the age of the star has come down significantly. Figure 12 compares the observed helium glitch signature with the corresponding signatures in the best-fit model frequencies. As we may expect from the too small surface helium abundance in the best-fit model obtained using *SeismicFit1*, the amplitude of the helium signature is smaller than the corresponding observed amplitude. The amplitude of the helium signature in the model frequencies obtained using *GlitchFit* is in better agreement with the observed one, particularly the amplitude averaged over the frequency range (better tracer of the helium abundance) are in much better agreement.

6.3. *KIC 6106415*

There are several stars in the LEGACY sample for which the results do not change on including the glitch parameters in the stellar model fitting. KIC 6106415 is an example of such a star. The results for this star are listed in the fifth and sixth rows of Table 2, and are consistent with the results of earlier works (see, Silva Aguirre et al. 2013). The numbers in the two rows are exactly the same because the best-fit models using two approaches turned out to be the same. Note from Table 2 that the masses, radii, and the ages were off only by about 2σ in the cases where secondary minimum was picked up by the *SeismicFit1* approach. This, in a way, justifies the other methods, which use only the spectroscopic and seismic data in the stellar model fitting.

7. CONCLUSIONS

We fitted the signatures of the acoustic glitches in the oscillation frequencies of 66 main-sequence stars observed by *Kepler* satellite using two different methods, and derived the acoustic depths of the base of the convection zone and helium ionization zone. We found that the signature from the He glitch is strong and the corresponding fit is robust for all stars, while the fit to the signature from the base of the convection zone is generally robust for the solar and sub-solar mass stars, but it is difficult to reliably fit its signature for super-solar mass stars. We fitted two different sets of best-fit model frequencies for all stars, and confirmed the findings of Broomhall et al. (2014) and Verma et al. (2014a) for the models of real stars that the fitted acoustic depth of the helium ionization zone correspond to the peak in the first adiabatic index between the first and second helium ionization zones.

We used the parameters associated with the helium glitch (average amplitude, width, and acoustic depth) together with the spectroscopic and seismic observables in the stellar model fitting to determine the stellar properties. The inclusion of the He glitch parameters puts tighter constraints on the stellar models, particularly on the initial helium abundance, and leads to a relatively more accurate set of stellar properties. This was demonstrated explicitly for the Sun-as-a-star and KIC 8760414 by modeling them with and without the information from the glitch analysis. There are other stars in the sample with the bimodal distribution of chi-square (similar to what is shown in Figure 10), for which the information from the glitch analysis helps constrain their properties better.

We studied the dependence of the various glitch parameters on the stellar parameters in the spirit of ensemble asteroseismology. We found that the acoustic depths of the base of the convection zone and helium ionization zone are positively correlated. Since the determination of $\tau_{\rm He}$ is reliable, we propose that the correlation be used as a guide to pick up the correct peak in the distribution of $\tau_{\rm CZ}$ (see, Figure 2 and 3), in cases when it has multiple peaks. The average amplitude of the helium signature increases not only with the helium abundance but also with the mass (hence the effective temperature), therefore a careful calibration is required to estimate the envelope helium abundance. The helium abundance obtained using the information from the glitch analysis is expected to be more reliable, and a detailed analysis using different methods, including its determination from the calibration of the observed average amplitude of the helium signature, will be presented in future.

Funding for the Stellar Astrophysics Centre is provided by The Danish National Research Foundation (Grant DNRF106). The research was supported by the ASTERISK project (ASTERoseismic Investigations with SONG and Kepler) funded by the European Research Council (Grant agreement no.: 267864). Authors thank J. Christensen-Dalsgaard and G. Houdek for a careful reading of the manuscript. KV thanks S. M. Chitre for his support at CEBS, where the first draft of the paper was written. KR and AM acknowledge support from the NIUS program of HBCSE (TIFR). SB is partially supported by NSF grant AST-1514676 and NASA grant NNX16A109G. MNL acknowledges the support of The Danish Council for Independent Research — Natural Science (Grant DFF-4181-00415). VSA acknowledges support from VILLUM FONDEN (research grant 10118).

REFERENCES

Adelberger, E. G., Austin, S. M., Bahcall, J. N., et al. 1998, Reviews of Modern Physics, 70, 1265
Aerts, C., Christensen-Dalsgaard, J., & Kurtz, D. W. 2010, Asteroseismology (Springer-Verlag, Heidelberg)
Angulo, C., Arnould, M., Rayet, M., et al. 1999, Nuclear Physics A, 656, 3
Asplund, M., Grevesse, N., Sauval, A. J., & Scott, P. 2009, ARA&A, 47, 481
Badnell, N. R., Bautista, M. A., Butler, K., et al. 2005, MNRAS, 360, 458
Baglin, A. 2006, in ESA Special Publication, Vol. 1306, The CoRoT Mission Pre-Launch Status - Stellar Seismology and Planet Finding, ed. M. Fridlund, A. Baglin, J. Lochard, & L. Conroy, 111
Baglin, A., Auvergne, M., Barge, P., et al. 2009, in IAU Symposium, Vol. 253, IAU Symposium, ed. F. Pont, D. Sasselov, & M. J. Holman, 71–81
Bailey, J. E., Nagayama, T., Loisel, G. P., et al. 2015, Nature, 517, 56
Ball, W. H., & Gizon, L. 2014, A&A, 568, A123
Balmforth, N. J., & Gough, D. O. 1990, ApJ, 362, 256
Basu, S. 1998, MNRAS, 298, 719

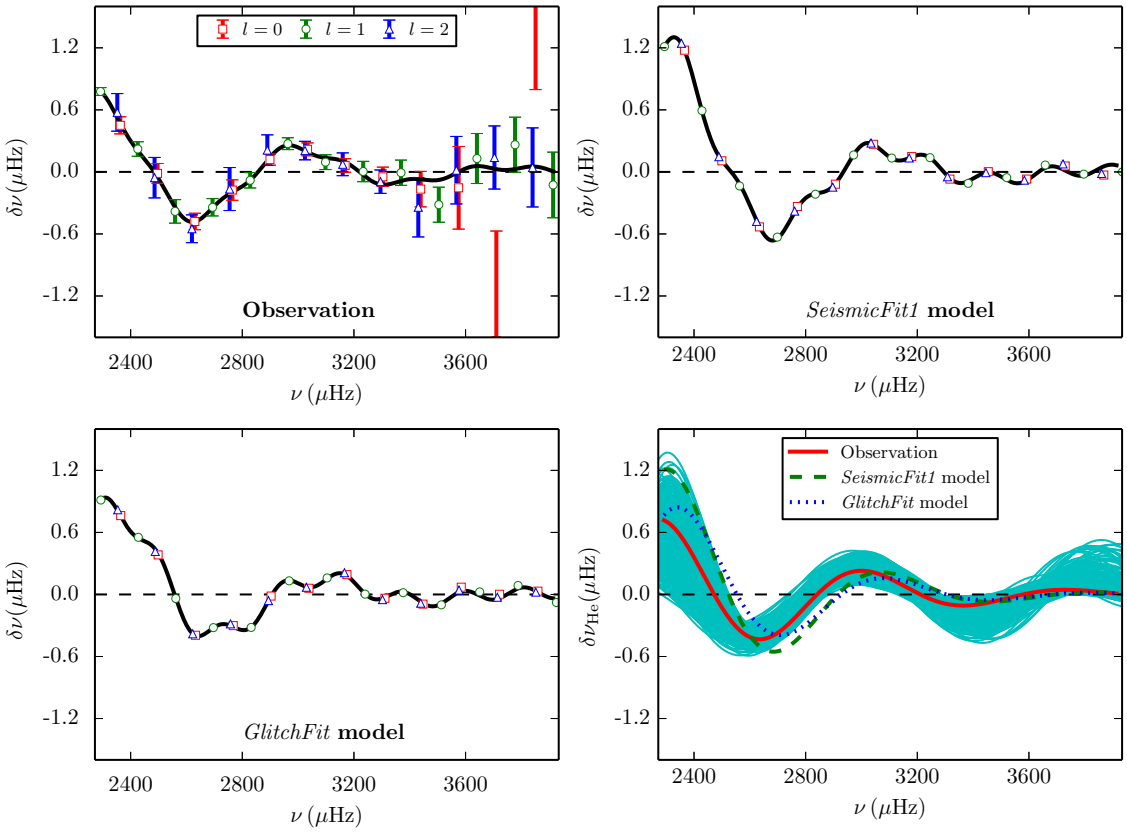

FIG. 11.— Fit to the observed and best-fit model frequencies of Sun-as-a-star. The top left panel shows the fit to the observed frequencies, while the top right and bottom left panels show the fits to the best-fit model frequencies. The bottom right panel shows the corresponding helium glitch signatures. The helium signatures in the cyan color correspond to the fits to 500 realizations of the observed frequencies.

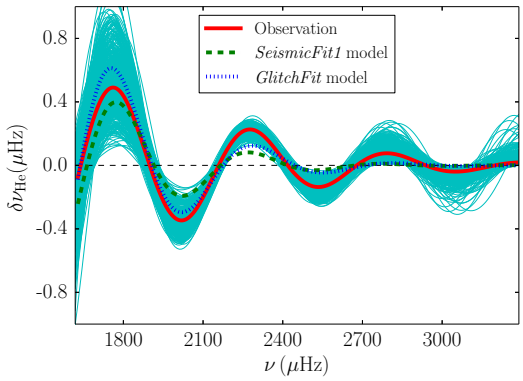

FIG. 12.— Helium glitch signature in the observed and best-fit model frequencies of KIC 8760414. The helium signatures in the cyan color correspond to the fits to 500 realizations of the observed frequencies.

Basu, S., & Antia, H. M. 2008, Phys. Rep., 457, 217
Basu, S., Antia, H. M., & Narasimha, D. 1994, MNRAS, 267, 209
Basu, S., Chaplin, W. J., & Elsworth, Y. 2010, ApJ, 710, 1596
Basu, S., Mazumdar, A., Antia, H. M., & Demarque, P. 2004, MNRAS, 350, 277
Bellinger, E. P., Angelou, G. C., Hekker, S., et al. 2016, ArXiv e-prints, arXiv:1607.02137
Borucki, W., Koch, D., Batalha, N., et al. 2009, in IAU Symposium, Vol. 253, IAU Symposium, ed. F. Pont, D. Sasselov, & M. J. Holman, 289–299
Broomhall, A.-M., Miglio, A., Montalbán, J., et al. 2014, MNRAS, 440, 1828
Casagrande, L., Silva Aguirre, V., Stello, D., et al. 2014, ApJ, 787, 110
Casagrande, L., Silva Aguirre, V., Schlesinger, K. J., et al. 2016, MNRAS, 455, 987
Chaplin, W. J., Kjeldsen, H., Christensen-Dalsgaard, J., et al. 2011, Science, 332, 213
Chaplin, W. J., Basu, S., Huber, D., et al. 2014, ApJS, 210, 1
Christensen-Dalsgaard, J. 2008, Ap&SS, 316, 113
Christensen-Dalsgaard, J., Gough, D. O., & Thompson, M. J. 1991, ApJ, 378, 413
Cox, J., & Giuli, R. 1968, Principles of Stellar Structure: Physical principles, Principles of Stellar Structure No. v. 1 (Gordon and Breach)
Demarque, P., Guenther, D. B., Li, L. H., Mazumdar, A., & Straka, C. W. 2008, Ap&SS, 316, 31
Ferguson, J. W., Alexander, D. R., Allard, F., et al. 2005, ApJ, 623, 585
Formicola, A., Imbriani, G., Costantini, H., et al. 2004, Physics Letters B, 591, 61
Gai, N., Basu, S., Chaplin, W. J., & Elsworth, Y. 2011, ApJ, 730, 63
Gilliland, R. L., Marcy, G. W., Rowe, J. F., et al. 2013, ApJ, 766, 40
Gough, D. 2013, Sol. Phys., 287, 9
Gough, D. O. 1990, in Lecture Notes in Physics, Berlin Springer Verlag, Vol. 367, Progress of Seismology of the Sun and Stars, ed. Y. Osaki & H. Shibahashi, 283
Gough, D. O. 2002, in ESA Special Publication, Vol. 485, Stellar Structure and Habitable Planet Finding, ed. B. Battrick, F. Favata, I. W. Roxburgh, & D. Galadi, 65–73
Gough, D. O., & Thompson, M. J. 1988, in IAU Symposium, Vol. 123, Advances in Helio- and Asteroseismology, ed. J. Christensen-Dalsgaard & S. Frandsen, 155
Grevesse, N., & Sauval, A. J. 1998, Space Sci. Rev., 85, 161

Gruberbauer, M., Guenther, D. B., & Kallinger, T. 2012, ApJ, 749, 109
Herwig, F. 2000, A&A, 360, 952
Houdek, G., & Gough, D. O. 2007, MNRAS, 375, 861
Iglesias, C. A., & Rogers, F. J. 1996, ApJ, 464, 943
Imbriani, G., Costantini, H., Formicola, A., et al. 2005, European Physical Journal A, 25, 455
Kjeldsen, H., Bedding, T. R., & Christensen-Dalsgaard, J. 2008, ApJ, 683, L175
Koch, D. G., Borucki, W. J., Basri, G., et al. 2010, ApJ, 713, L79
Kunz, R., Fey, M., Jaeger, M., et al. 2002, ApJ, 567, 643
Lebreton, Y., & Goupil, M. J. 2014, A&A, 569, A21
Liu, K., Bi, S.-L., Li, T.-D., et al. 2014, Research in Astronomy and Astrophysics, 14, 1447
Lopes, I. P., & Gough, D. 2001, MNRAS, 322, 473
Lund, M. N., Silva Aguirre, V., Davies, G. R., et al. 2016, ApJ(accepted), arXiv:1612.00436
Mathur, S., Metcalfe, T. S., Woitaszek, M., et al. 2012, ApJ, 749, 152
Mazumdar, A. 2005, A&A, 441, 1079
Mazumdar, A., & Antia, H. M. 2001, A&A, 377, 192
Mazumdar, A., Michel, E., Antia, H. M., & Deheuvels, S. 2011, in Transiting Planets, Vibrating Stars and Their Connection, ed. A. Baglin, M. Deleuil, E. Michel, C. Moutou, & T. Seman, Proceedings of Second *CoRoT* Symposium, 197
Mazumdar, A., Michel, E., Antia, H. M., & Deheuvels, S. 2012, A&A, 540, A31
Mazumdar, A., Singhal, L., & Prabhu, S. 2010, Astronomische Nachrichten, 331, 961
Mazumdar, A., Monteiro, M. J. P. F. G., Ballot, J., et al. 2014, ApJ, 782, 18
Metcalfe, T. S., Creevey, O. L., & Christensen-Dalsgaard, J. 2009, ApJ, 699, 373
Metcalfe, T. S., Creevey, O. L., Doğan, G., et al. 2014, ApJS, 214, 27
Miglio, A., Montalbán, J., Carrier, F., et al. 2010, A&A, 520, L6
Miglio, A., Chiappini, C., Morel, T., et al. 2013, MNRAS, 429, 423
Monteiro, M. J. P. F. G., Christensen-Dalsgaard, J., & Thompson, M. J. 1994, A&A, 283, 247
—. 2000, MNRAS, 316, 165
Monteiro, M. J. P. F. G., & Thompson, M. J. 1998, in IAU Symposium, Vol. 185, New Eyes to See Inside the Sun and Stars, ed. F.-L. Deubner, J. Christensen-Dalsgaard, & D. Kurtz, 317
Monteiro, M. J. P. F. G., & Thompson, M. J. 2005, MNRAS, 361, 1187
Nutzman, P., Gilliland, R. L., McCullough, P. R., et al. 2011, ApJ, 726, 3
Paxton, B., Bildsten, L., Dotter, A., et al. 2011, ApJS, 192, 3
Paxton, B., Cantiello, M., Arras, P., et al. 2013, ApJS, 208, 4
Planck Collaboration, Ade, P. A. R., Aghanim, N., et al. 2016, A&A, 594, A13
Reese, D. R., Chaplin, W. J., Davies, G. R., et al. 2016, A&A, 592, A14
Rogers, F. J., & Nayfonov, A. 2002, ApJ, 576, 1064
Roxburgh, I. W. 2011, in Transiting Planets, Vibrating Stars and Their Connection, ed. A. Baglin, M. Deleuil, E. Michel, C. Moutou, & T. Seman, Proceedings of Second *CoRoT* Symposium, 161
Roxburgh, I. W., & Vorontsov, S. V. 2003, A&A, 411, 215
Seaton, M. J. 2005, MNRAS, 362, L1
Silva Aguirre, V., Basu, S., Brandão, I. M., et al. 2013, ApJ, 769, 141
Silva Aguirre, V., Davies, G. R., Basu, S., et al. 2015, MNRAS, 452, 2127
Silva Aguirre, V., Lund, M. N., Antia, H. M., et al. 2016, ApJ(accepted), arXiv:1611.08776
Steigman, G. 2010, JCAP, 4, 029
Tassoul, M. 1980, ApJS, 43, 469
Thoul, A. A., Bahcall, J. N., & Loeb, A. 1994, ApJ, 421, 828
Verma, K., Antia, H. M., Basu, S., & Mazumdar, A. 2014a, ApJ, 794, 114
Verma, K., Hanasoge, S., Bhattacharya, J., Antia, H. M., & Krishnamurthi, G. 2016, MNRAS, 461, 4206
Verma, K., Faria, J. P., Antia, H. M., et al. 2014b, ApJ, 790, 138
Vorontsov, S. V. 1988, in IAU Symposium, Vol. 123, Advances in Helio- and Asteroseismology, ed. J. Christensen-Dalsgaard & S. Frandsen, 151